Chinese Physics Letters **41**, 066801 (2024)

Layer-Valley Hall Effect under Inversion and Time-Reversal Symmetries

Jiaojiao Zhao(赵交交)[1,2], Gui-Bin Liu(刘贵斌)[3,4*], Peng Chen(陈鹏)[5], Yugui Yao(姚裕贵)[3,4], Guangyu Zhang(张广宇)[1,2,6], and Luojun Du(杜罗军)[1,2*]

[1]*Beijing National Laboratory for Condensed Matter Physics, and Key Laboratory for Nanoscale Physics and Devices, Institute of Physics, Chinese Academy of Sciences, Beijing 100190, China*
[2]*School of Physical Sciences, University of Chinese Academy of Sciences, Beijing 100190, China*
[3]*Centre for Quantum Physics, Key Laboratory of Advanced Optoelectronic Quantum Architecture and Measurement (MOE), School of Physics, Beijing Institute of Technology, Beijing 100081, China*
[4]*Beijing Key Lab of Nanophotonics & Ultrafine Optoelectronic Systems, School of Physics, Beijing Institute of Technology, Beijing 100081, China*
[5]*Schoolof Microelectronics, Southern University of Science and Technology, Shenzhen 518055, China*
[6]*Songshan Lake Materials Laboratory, Dongguan 523808, China*

(Received 28 March 2024; accepted manuscript online 23 May 2024)

Hall effects have been the central paradigms in modern physics, materials science and practical applications, and have led to many exciting breakthroughs, including the discovery of topological Chern invariants and the revolution of metrological resistance standard. To date, the Hall effects have mainly focused on a single degree of freedom (DoF), and most of them require the breaking of spatial-inversion and/or time-reversal symmetries. Here we demonstrate a new type of Hall effect, i.e., layer-valley Hall effect, based on a combined layer-valley DoF characterized by the product of layer and valley indices. The layer-valley Hall effect has a quantum origin arising from the layer-valley contrasting Berry curvature, and can occur in nonmagnetic centrosymmetric crystals with both spatial-inversion and time-reversal symmetries, transcending the symmetry constraints of single DoF Hall effect based on the constituent layer or valley index. Moreover, the layer-valley Hall effect is highly tunable and shows a W-shaped pattern in response to the out-of-plane electric fields. Additionally, we discuss the potential detection approaches and material-specific design principles of layer-valley Hall effect. Our results demonstrate novel Hall physics and open up exotic paradigms for new research direction of layer-valleytronics that exploits the quantum nature of the coupled layer-valley DoF.

DOI: 10.1088/0256-307X/41/6/066801

The Hall effect, first discovered by Edwin Hall in 1879, refers to a transverse conductivity generated in response to a longitudinal driving current and has been a central theme in condensed-matter physics and materials science.[1,2] The study of Hall effects has strongly advanced our understanding of fundamental physical properties (e.g., fractional statistics, topological and geometrical properties of Bloch wavefunctions) and substantially transformed the landscape of technological innovations (such as magnetic field measurements, metrological resistance standard, and topological quantum computing).[2–9] To date, the Hall effects have mainly focused on a single internal degree of freedom (DoF) of electrons/holes, such as charge DoF (ordinary Hall effect and nonlinear Hall effect), spin DoF (spin Hall effect), valley DoF (valley Hall effect), and layer DoF (layer Hall effect).[6,10–17] Typically, most Hall effects based on a single DoF require the breaking of spatial-inversion and/or time-reversal symmetries. For example, ordinary Hall effect results from broken time-reversal symmetry;[18] valley and nonlinear Hall effects are associated with spatial-inversion symmetry breaking;[6,10,11,19] layer Hall effect are intricately connected with the breaking of both spatial-inversion and time-reversal symmetries.[12,14] Remarkably, for a system with multiple intrinsic DoFs, combined DoFs characterized by the product of two or more single DoFs may emerge. For example, a combined spin-valley DoF characterized by the product of spin and valley indices has been demonstrated in an antiferromagnetic honeycomb lattice.[20] The combined DoF characterized by the product of multiple DoFs can potentially open up a new paradigm for emergent Hall effects, which may enable unprecedented capabilities to transcend the symmetry constraints of single DoF Hall effects and to underpin exotic physics inaccessible in Hall effects based on a single DoF.

In this work, we demonstrate a new type of Hall effect, i.e., the layer-valley Hall effect, based on a combined layer-valley DoF characterized by the product of layer and valley indices, in which electrons/holes with opposite layer-valley indices spontaneously deflect in opposing transverse directions under a driving electric field. In stark contrast to most single DoF Hall effects that usually require particular symmetry breaking, the emergent layer-valley Hall effect can transcend the symmetry constraints and can occur

*Corresponding authors. Email: luojun.du@iphy.ac.cn; gbliu@bit.edu.cn

under both spatial-inversion and time-reversal symmetric conditions. Moreover, the layer-valley Hall effect has a quantum origin arising from the layer-valley contrasting Berry curvature and can be dynamically continually tuned by external fields, showing a W-shaped pattern. In addition, we discuss three potential detection approaches and the material-specific design principles of layer-valley Hall effect.

The $\boldsymbol{k}\cdot\boldsymbol{p}$ Model of Bilayer TMDCs. Here, we choose nonmagnetic centrosymmetric bilayer transition metal dichalcogenides (TMDCs) with thermodynamically favorable 2H stacking order, in which internal quantum layer and valley DoFs exist simultaneously,[21] to demystify the emergent layer-valley Hall effect under both inversion and time-reversal symmetric conditions. In contrast to monolayer TMDCs where inversion symmetry is explicitly broken, the 180° in-plane rotation between the upper- and lower-layers results in the restoration of inversion symmetry in bilayer TMDCs of 2H stacking with point group symmetry $D_{3\mathrm{d}}$ [Fig. 1(a)]. Correspondingly, the effective $\boldsymbol{k}\cdot\boldsymbol{p}$ Hamiltonian of inversion-symmetric bilayer TMDCs in the neighborhood of $\pm K$ valleys can be written as[22–24]

$$H(k)=\begin{bmatrix} \Delta & 0 & \xi_{13} & 0 \\ 0 & \Delta & 0 & \xi_{24} \\ \xi_{31} & 0 & \tau s_z\lambda & t_\perp \\ 0 & \xi_{42} & t_\perp & -\tau s_z\lambda \end{bmatrix}, \tag{1}$$

with

$$\xi_{13}=at(\tau k_x+ik_y),\quad \xi_{24}=at(\tau k_x-ik_y),$$
$$\xi_{31}=at(\tau k_x-ik_y),\quad \xi_{42}=at(\tau k_x+ik_y).$$

Here $\{|d^u_{z^2}\rangle,\ |d^l_{z^2}\rangle,\ \frac{1}{\sqrt{2}}(|d^u_{x^2-y^2}\rangle+i\tau|d^u_{xy}\rangle),\ \frac{1}{\sqrt{2}}(|d^l_{x^2-y^2}\rangle-i\tau|d^l_{xy}\rangle)\}$ is the basis with superscripts u and l denoting the noncentrosymmetric upper and lower layers, respectively. Δ is the monolayer bandgap, a indicates the lattice constant, $\boldsymbol{k}$ represents the relative wavevector with respect to the $\pm K$ points, t is the nearest-neighbor intra-layer hopping integral, λ represents the spin–orbit coupling of valence bands, $t_\perp$ denotes the interlayer hopping for holes, $\tau=\pm1$ is the valley index ($1/-1$ for $K/-K$), and $s_z=\pm1$ indicates spin-up/spin-down states. It is noteworthy that the interlayer hopping vanishes at the conduction band edge of $\pm K$ points because of the combination of C_3 rotational symmetry and d_{z^2} orbital nature.[24]

Layer-Valley Hall Effect of Holes in Uncoupled Bilayer TMDCs. In the light of the $\boldsymbol{k}\cdot\boldsymbol{p}$ Hamiltonian (1), the four energetically degenerate eigenstates at the higher lying states of valence band edge of bilayer TMDCs are:

$$|\tau,s_z\rangle=\beta_u\left(\left|d^u_{x^2-y^2}\right\rangle+i\tau\left|d^u_{xy}\right\rangle\right)+\beta_l\left(\left|d^l_{x^2-y^2}\right\rangle-i\tau\left|d^l_{xy}\right\rangle\right), \tag{2}$$

where $|\beta_u|^2=\frac{1}{2}+\tau s_z\frac{\lambda}{2\sqrt{\lambda^2+t_\perp^2}}$ ($|\beta_l|^2=\frac{1}{2}-\tau s_z\frac{\lambda}{2\sqrt{\lambda^2+t_\perp^2}}$) represents the probability of the constituent upper (lower) layer.[22,25] Correspondingly, the layer polarization of eigenstates $|\tau,\ s_z\rangle$ is $\rho=\frac{|\beta_u|^2-|\beta_l|^2}{|\beta_u|^2+|\beta_l|^2}=\tau s_z\frac{\lambda}{\sqrt{\lambda^2+t_\perp^2}}$. $\rho=\sim1$ ($\rho=\sim-1$) indicates that eigenstates $|\tau,\ s_z\rangle$ are spatially localized in upper (lower) layer and thus harbor a quantum layer DoF of $\kappa=1$ ($\kappa=-1$).[21,22] Here we focus only on the top valence bands, the lower lying ones are hundreds of meV away and are therefore ignored [Fig. 1(b)].

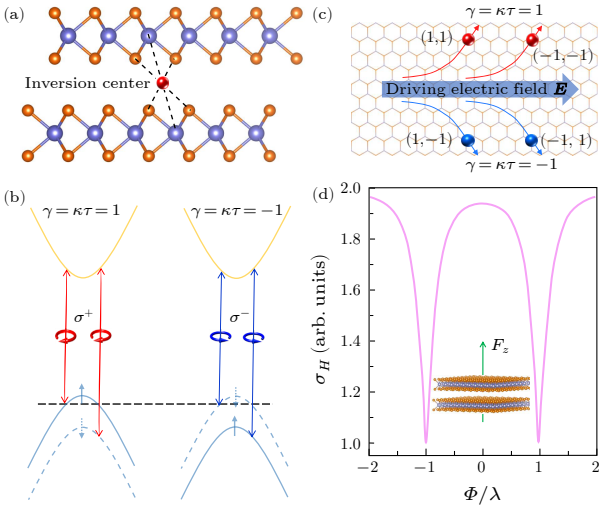

Fig. 1. Tunable layer-valley Hall effect in nonmagnetic centrosymmetric bilayer TMDCs. (a) Side view of 2H stacked bilayer TMDCs. Because of the 180° in-plane rotation between the upper and lower layers, inversion symmetry is present in bilayer TMDCs of 2H stacking. (b) Schematics representing the layer-valley dependent optical dipole selection rules. Here σ^+ (σ^-) denotes left (right) circularly polarized light. Valence band shows spin–orbit splitting in hundreds of meV. Spin configurations are indicated by solid ↑ (spin-up) and dotted ↓ (spin-down). (c) Illustration of the layer-valley Hall effect. Upon applying a driving electric field, electrons/holes with opposite layer-valley indices spontaneously deflect in opposing transverse directions. The layer and valley indices, (κ, τ), are indicated in parentheses. (d) The layer-valley Hall conductivity of bilayer TMDCs as a function of Φ/λ. Φ (λ) is the potential difference between the upper and lower layers (spin–orbit coupling of valence band). Inset: schematic illustration of bilayer TMDC with an out-of-plane displacement field.

First, we consider the ideal, uncoupled bilayer TMDC crystals. Note that the point group symmetry of uncoupled bilayer TMDCs still belongs to the centrosymmetric $D_{3\mathrm{d}}$. Owing to the decoupled nature (that is, $t_\perp$ is zero), $\rho=1$ ($\rho=-1$) for eigenstates $|\tau,\ s_z\rangle$ with $\tau s_z=1$ ($\tau s_z=-1$). This indicates that eigenstates $|\tau,\ s_z\rangle$ with $\tau s_z=1$ ($\tau s_z=-1$) are 100% localized in upper (lower) layer and show a layer DoF of $\kappa=1$ ($\kappa=-1$). Because of the full layer localization, it is easily conceivable that each $|\tau,\ s_z\rangle$ in uncoupled centrosymmetric bilayer TMDCs would inherit the nonvanishing Berry curvature Ω from the constituent upper or lower layer, where the inversion symmetry is intrinsically broken. Quantitatively, the Berry curvature associated with Bloch eigenstate $|\tau,\ s_z\rangle$ in uncoupled bilayer TMDCs is $\Omega(\tau,\ s_z)=\nabla_{\boldsymbol{k}}\times\langle\tau,\ s_z|i\nabla_{\boldsymbol{k}}|\tau,\ s_z\rangle=\kappa\tau\Omega_{\mathrm{I}}$, where $\Omega_{\mathrm{I}}\approx\frac{2a^2t^2}{(\Delta-\lambda)^2}$ denotes the magnitude of Berry curvature in the neighborhood of $\pm K$ valleys of monolayer TMDCs.[11] Strikingly, the Berry curvature in inversion-symmetric, uncoupled bi-

layer TMDCs is nonvanishing and depends on the product of layer and valley indices. Therefore, a combined layer-valley DoF of $\gamma = \kappa\tau$ and layer-valley contrasting Berry curvature can be identified in uncoupled bilayer TMDCs. This bears striking resemblance to the combined spin-valley DoF and spin-valley dependent Berry curvature previously demonstrated.[20] It is noteworthy that for layer-valley contrasting Berry curvature in uncoupled bilayer TMDCs, the Berry curvature from upper and lower layers is compensated by each other for a given valley and hence the net Berry curvature remains zero, as imposed by the global inversion symmetry and time reversal symmetry.

The presence of nonvanishing layer-valley Berry curvature, which can be viewed as an internal pseudo-magnetic field in momentum space, would significantly modify the carrier dynamics and result in new topological transport phenomena.[3] In particular, under an applied electric field $\boldsymbol{E}$, the Berry curvature can drive an anomalous transverse velocity $\boldsymbol{v} = \frac{e}{\hbar}\boldsymbol{E} \times \boldsymbol{\Omega}(\boldsymbol{k})$, where e is the elementary charge and $\hbar$ denotes the reduced Planck constant.[3,21] Because of the layer-valley contrasting Berry curvature, carriers with opposite layer-valley indices flow in opposing transverse directions under an external electric field, resulting in the layer-valley Hall effect [Fig. 1(c)]. Quantitatively, for moderate hole doping with chemical potential lying between the two-split valence-bands [illustrated by the dashed line in Fig. 1(b)], the layer-valley Hall conductivity (in units of $e/\hbar$) is given by[11]

$$\begin{aligned}\sigma_{\mathrm{H}} &= 2\int_{BZ}\frac{d^2\boldsymbol{k}}{(2\pi)^2}\left[f_{\uparrow}(\boldsymbol{k})\,\boldsymbol{\Omega}_{\uparrow}\ (\boldsymbol{k}) + f_{\downarrow}(\boldsymbol{k})\,\boldsymbol{\Omega}_{\downarrow}(\boldsymbol{k})\right] \\ &= \frac{2}{\pi}\frac{\mu}{\Delta-\lambda},\end{aligned} \tag{3}$$

where $f(\boldsymbol{k})$ is the equilibrium Fermi–Dirac distribution, μ is the Fermi energy measured from the valence-band maximum, and the integration is performed over the states with layer-valley DoF of $\gamma = 1$. Here we focus only the intrinsic layer-valley Hall effect with the Berry curvature contribution, while ignoring the contributions from side-jump, skew-scattering and other mechanisms due to intervalley scattering.[2,26] Notably, the layer-valley Hall conductivity in uncoupled bilayer TMDCs is twice the monolayer valley Hall conductivity. This can be understood intuitively as that for the layer-valley Hall conductivity contributed from a given layer-valley index (such as $\gamma = \kappa\tau = 1$), there are two contributions of equal magnitude to monolayer valley Hall conductivity: one from K valley of upper layer ($\tau = 1$, $\kappa = 1$) and the other from $-K$ valley of lower layer ($\tau = -1$, $\kappa = -1$) [Fig. 1(c)]. Because of the superposition of these two contributions, layer-valley Hall effect exhibits a doubling of conductivity response. In addition, we point out that in the layer-valley Hall effect, carriers in the K ($-K$) valley of the upper layer and $-K$ (K) of lower layer flow in the same transverse direction, the net valley Hall effect remains zero, as imposed by the global inversion symmetry.[10,11,27]

In close resemblance to the coupled valley and spin DoFs in the valence band of monolayer TMDCs,[11] the combined layer-valley DoF is coupled with spin DoF in bilayer TMDCs. Specifically, for top valence bands, the layer-valley configurations $\gamma = \kappa\tau = 1/-1$ are coupled exclusively with spin-up/spin-down. Because of the strong coupling between the combined layer-valley and spin DoFs, layer-valley Hall effect is accompanied by an intrinsic spin Hall effect with the same magnitude (see the Supplementary Information).

Layer-Valley Hall Effect of Electrons in Uncoupled Bilayer TMDCs. In akin to valence band case, each eigenstate $|\tau, s_z\rangle$ of conduction bands in uncoupled bilayer TMDCs is also 100% localized in either upper or lower layer, and shows layer-valley contrasting Berry curvature $\boldsymbol{\Omega}$: $\Omega_{\mathrm{c}}(\tau, s_z) = -\kappa\tau\Omega_{\mathrm{I}}$ (see the Supplementary Information). For a given layer-valley index, the Berry curvature of conduction band is opposite to that of valence band. The layer-valley contrasting Berry curvature in conduction bands would give rise to layer-valley Hall effect for electrons. Quantitatively, the layer-valley Hall conductivity (in units of $e/\hbar$) for moderate electron doping in uncoupled bilayer TMDCs is $\sigma^{e}_{\mathrm{H}} = \frac{2}{\pi}\frac{\mu\Delta}{\Delta^2-\lambda^2}$, where μ is the Fermi energy measured from the conduction-band minimum (see the Supplementary Information). Although layer-valley Hall effect of electrons is also accompanied by a spin Hall effect, the spin Hall conductivity shows a much smaller magnitude and is about λ/Δ of the layer-valley Hall conductivity, for instance λ/Δ is only $\sim 4\%$ for bilayer MoS_2 (see the Supplementary Information). The much smaller spin Hall conductivity is due to the fact that the spin DoF is decoupled with the layer-valley DoF at the conduction band-edge and for a given layer-valley index γ with fixed layer (valley) index κ (τ), both spin-up and spin-down states need to be taken into account (see the Supplementary Information).

Tunable Layer-Valley Hall Effect in Real Bilayer TMDCs. For electrons in conduction bands, real bilayer TMDCs would show layer-valley Hall effect as in the uncoupled cases, because of the vanishing interlayer hopping.[22,24,25] We therefore focus on the layer-valley Hall effect of holes in valence bands of real bilayer TMDCs, where nonvanishing interlayer hopping exists. Remarkably, due to the giant spin–orbit coupling of the d orbitals of the transition metal atoms, $t_{\perp}$ is much smaller than λ and the interlayer hopping is virtually suppressed. As a consequence, each branch of the four-fold degenerate eigenstates at the top valence band of real bilayer TMDCs exhibits a close-to-unity layer polarization ρ (for instance, the layer polarization of bilayer WS_2 is $\rho = \pm 0.96$).[22,25,28] This indicates that eigenstates $|\tau, s_z\rangle$ with $\tau s_z = 1$ ($\tau s_z = -1$) are spatially localized in upper (lower) layer and harbor a layer DoF of $\kappa = 1$ ($\kappa = -1$). In resemblance to uncoupled bilayer TMDCs, the layer polarized eigenstates in real bilayer TMDCs would enable layer-valley contrasting Berry curvature: $\Omega(\tau, s_z) = \kappa\tau|\rho|\Omega_{\mathrm{I}}$. Note that the layer-valley contrasting Berry curvature has been determined in inversion-symmetric WSe_2 by angle-resolved photoelectron spectroscopy technique with high surface sensitivity.[29] The layer-valley contrasting Berry curvature would give rise to exotic layer-valley Hall effect in

real bilayer TMDCs with conductivity of $\sigma_{\rm H} = \frac{2|\rho|}{\pi}\frac{\mu}{\Delta-\lambda}$. Compared to the results of uncoupled bilayer TMDCs, the Berry curvature and layer-valley Hall conductivity of real bilayer TMDCs are simply multiplied by a close-to-unity layer polarization factor $|\rho|$.

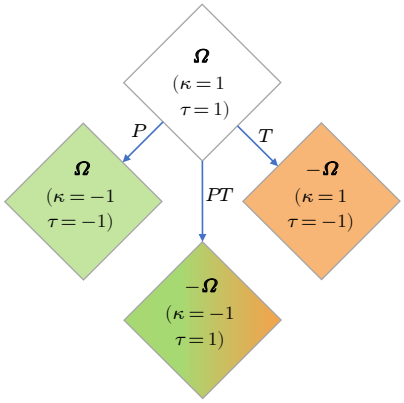

Fig. 2. Constraints of spatial-inversion and time-reversal symmetries on Berry curvature Ω. P: inversion symmetry; T: time-reversal symmetry; PT: space-time symmetry.

Because layer polarization can be controlled through external means, such as electric fields and pressure engineering, layer-valley Hall effects in real bilayer TMDCs show high tunability.[25,30,31] For example, pressure can strengthen the interlayer hopping $t_\perp$, leading to a monotonic decrease in layer polarization and layer-valley Hall conductivity. Upon applying an out-of-plane displacement field F_z, a potential difference (i.e., $2\Phi = eF_z d$, d denotes the interlayer separation) appears between the upper and lower layers.[25,32]. Consequently, the energy cost for interlayer hopping changes from λ to $\lambda + \tau s_z \Phi$, and thus layer polarization becomes $\rho = \tau s_z \frac{\lambda+\tau s_z\Phi}{\sqrt{(\lambda+\tau s_z\Phi)^2+t_\perp^2}}$ (Ref. [25]). Correspondingly, the electric field dependent layer-valley Hall conductivity (in units of $e/\hbar$) is

$$\sigma_{\rm H} = \frac{1}{\pi}\frac{\mu}{\Delta-\lambda_v}\left[\frac{\lambda+\Phi}{\sqrt{(\lambda+\Phi)^2+t_\perp^2}} + \frac{\lambda-\Phi}{\sqrt{(\lambda-\Phi)^2+t_\perp^2}}\right]. \tag{4}$$

Figure 1(d) presents the layer-valley Hall conductivity of bilayer TMDCs as a function of potential difference Φ. With increasing the potential difference Φ, the layer-valley Hall conductivity first decreases and then increases, showing a W-shaped pattern with the minimum at $\Phi = \lambda$. In contrast to the valley Hall effect in non-centrosymmetric monolayer TMDCs, which cannot be easily tuned, the electric field-tunable layer-valley Hall effect in bilayer TMDCs represents an advantageous scenario for technological applications in next-generation electronics and optoelectronics. Further, we envision that layer-valley Hall effect could also be engineered by other external control, such as strain, pressure, and moiré engineering.[31,33,34]

Symmetry Insights of Layer-Valley Hall Effect. Interestingly, the novel Hall effect based on the combined layer-valley can emerge under both spatial-inversion and time-reversal symmetric conditions. This is in marked contrast to the single DoF Hall effects based on the constituent layer or valley index that require the breaking of spatial-inversion and/or time-reversal symmetries.[11,12] Here we show the general symmetry analysis to further illustrate this point. For system with both spatial-inversion and time-reversal symmetries, the Berry curvature should meet $\boldsymbol{\Omega}(\kappa=1,\tau=1) = \boldsymbol{\Omega}(\kappa=-1,\tau=-1) = -\boldsymbol{\Omega}(\kappa=1,\tau=-1) = -\boldsymbol{\Omega}(\kappa=-1,\tau=1)$ (Fig. 2). Clearly, layer-valley contrasting Berry curvature and thus layer-valley Hall effect can indeed exist. By contrast, for a given valley/layer, the net Berry curvature is null, resulting the absence of valley/layer Hall effect. This clearly shows that layer-valley Hall effect can transcend the symmetry constraints of single DoF Hall effects based on the constituent layer or valley index and occur in nonmagnetic centrosymmetric crystals with both spatial-inversion and time-reversal symmetries.

Detection of Layer-Valley Hall Effect. After elucidating the layer-valley Hall effect, here we demonstrate the feasible detection methods. Figure 3 shows three possible approaches for detecting the layer-valley Hall effect: nonlocal measurement method [Fig. 3(a)], Kerr rotation imaging approach [Fig. 3(b)], and optoelectronic method [Fig. 3(c)]. In the light of Onsager's reciprocity relations,[35] the nonvanishing Berry curvature responsible for layer-valley Hall effect would also ensure the inverse layer-valley Hall effect, an inverse process of layer-valley Hall effect that converts a nonzero layer-valley current into a transverse electric field (see the Supplementary Information). This generates the nonlocal resistance and nonlocal voltage, enabling the possibility of detecting layer-valley Hall effect with the nonlocal measurements shown in Fig. 3(a). Note that such a nonlocal Hall bar configuration has been widely used for probing the spin and valley Hall effects.[16,36]

In the layer-valley Hall effect, carriers with different layer-valley indices flow in opposite transverse directions, leading to an accumulation of layer-valley polarized carriers along the device channel edges [Fig. 3(b)]. Because carriers carry layer-valley contrasting orbital magnetic moments (see the Supplementary Information), a net layer-valley magnetization of opposing sign accumulates at the two edges of the sample. In akin to spin/valley magnetization,[16,37] such a layer-valley magnetization in principle, can lead to the polarization rotation of linearly polarized light and thus open the possibility of directly imaging layer-valley Hall effect via Kerr rotation microscopy [Fig. 3(b)]. Meanwhile, the layer-valley contrasting orbital magnetic moments can give rise to layer-valley dependent optical dipole selection rules. Specifically, the interband transitions associated with layer-valley DoF of $\gamma = \kappa\tau = 1$ (-1) are coupled exclusively with σ^+ (σ^-) circularly polarized optical field [Fig. 1(b), also see the Supplementary Information]. Note that such layer-valley dependent optical dipole selection rules have been experimentally demonstrated in bilayer TMDCs by circular polarization-resolved photoluminescence measurements.[23,38] Consequently, by shining circularly polarized light to create a population imbalance between opposite layer-valley DoFs and thus layer-valley

polarized carriers, layer-valley Hall effect would be evidenced as a measurable transverse voltage [Fig. 3(c)]. It is noteworthy that because of the layer-valley contrasting orbital magnetic moments, the layer-valley DoF can be manipulated by magnetic fields, representing an advantageous scenario for applications.

Recently, both Kerr rotation imaging experiments and nonlocal transport measurements have shown that centrosymmetric bilayer TMDCs (including boron nitride encapsulated high-quality devices) exhibit sizeable Kerr rotation/nonlocal signals even in the absence of external electric fields.[37,39] Though it was argued that such unexpected behavior could originate from substrate induced breaking of spatial-inversion symmetry (in fact, inversion symmetry should not be broken in the case of boron nitride encapsulation[40]), we highlight that layer-valley Hall effect is likely to be the underlying origin of the unexpected signals of inversion-symmetric bilayer TMDCs at zero electric field.

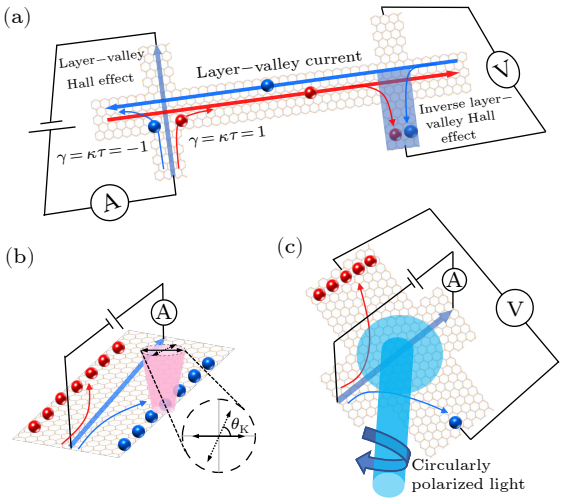

Fig. 3. Detection of layer-valley Hall effect. (a) Schematic of the nonlocal transport measurement of layer-valley Hall current. The driving electric field in the left-hand circuit generates a pure layer-valley current in the transverse direction by means of layer-valley Hall effect. Inverse layer-valley Hall effect then converts the layer-valley current into an electric field, generating the nonlocal resistance and nonlocal voltage in the right-hand circuit. (b) Schematic illustration of the Kerr rotation imaging approach. Under normal incidence of linearly polarized light, the accumulation of layer-valley polarized carriers along the channel edges enables the polarization rotation and measurable Kerr rotation θ_K of the reflected beam. (c) Illustration of the layer-valley Hall optoelectronic measurement. Photocarriers with particular layer-valley index are selectively excited by circularly polarized light, breaking the layer-valley degeneracy and resulting in a photoinduced anomalous Hall voltage.

Design Principles of Layer-Valley Hall Effect. It is conceivable that apart from bilayer TMDCs, the layer-valley Hall effect would also occur in a wide range of other nonmagnetic centrosymmetric crystals. Here we demonstrate the material-specific design principles that could aid future searches for potential candidates of layer-valley Hall effect. First, multiple degenerate but inequivalent local energy extrema exist in the conduction or valence bands, endowing the quantum valley DoF.[21] Second, the Bloch wavefunctions are localized in real-space sectors, enabling the layer DoF. For inversion-symmetric crystal, it consists of two local layers that are connected to each other through an inversion center. To ensure the layer DoF, the hybridization and entanglement of the wavefunctions between the two inversion-partner layers should be rather weak. Consequently, Bloch electrons associated with a particular wavefunctions at a given valley are spatially localized on one of the two inversion-partner layers and show the coupled layer-valley DoF. In the light of this design principle, we find that layered crystals with a small interaction or materials with a specific symmetry (such as nonsymmorphic symmetry which can enforce the wavefunction segregation) are promising candidates.[41–43] Third, the inversion symmetry of atomic site point group should be broken, so that the valley-contrasting Berry curvature can exist in each of the two inversion-partner layers. It is noteworthy that inversion symmetry breaking of site point group is a fundamental concept established recently and has revolutionized our understanding of spin-polarization effects and other physical phenomena (such as orbital polarization, piezoelectric polarization, Berry curvature, circular dichroism, and high-temperature superconductivity) in inversion-symmetric crystals.[28,29,41,43–47] Considering that out of the 32 point groups, 21 are noncentrosymmetric,[44,48] a large number of centrosymmetric materials could have inversion-asymmetric atomic site point groups and thus are promising candidates of layer-valley Hall effects.

In conclusion, we have demonstrated a completely new type of Hall effect, i.e., the layer-valley Hall effect. In contrast to the previously studied single DoF Hall effects, the layer-valley Hall effect is based on a combined layer-valley DoF characterized by the product of layer and valley indices. The layer-valley Hall effect has a quantum origin arising from the layer-valley contrasting Berry curvature, and can occur in systems with both spatial-inversion and time-reversal symmetries, transcending the symmetry constraints of most Hall effects based on the single DoF. Moreover, the layer-valley Hall effect is highly tunable with out-of-plane electric fields and shows a W-shaped pattern with the minimum at $\Phi = \lambda$. Our results open up new paradigms for topological quantum transport and will stimulate further studies to look for emergent Hall effects and technological innovations based on the combined DoFs.

Acknowledgments. This work was supported by the National Natural Science Foundation of China (Grant Nos. 61888102 and 12274447), the National Key Research and Development Program of China (Grant Nos. 2021YFA1202900 and 2023YFA1407000), the Key-Area Research and Development Program of Guangdong Province, China (Grant No. 2020B0101340001), the Guangdong Major Project of Basic and Applied Basic Research (Grant No. 2021B0301030002), and the Strategic Priority Research Program of Chinese Academy of Sci-

ences (CAS) (Grant No. XDB0470101).

References

[1] Hall E H 1879 *Am. J. Math.* **2** 287

[2] Nagaosa N, Sinova J, Onoda S, MacDonald A H, and Ong N P 2010 *Rev. Mod. Phys.* **82** 1539

[3] Xiao D, Chang M C, and Niu Q 2010 *Rev. Mod. Phys.* **82** 1959

[4] Feldman D E and Halperin B I 2021 *Rep. Prog. Phys.* **84** 076501

[5] von Klitzing K 2019 *Phys. Rev. Lett.* **122** 200001

[6] Du Z Z, Lu H Z, and Xie X C 2021 *Nat. Rev. Phys.* **3** 744

[7] Du L J, Hasan T, Castellanos-Gomez A, Liu G B, Yao Y G, Lau C N, and Sun Z P 2021 *Nat. Rev. Phys.* **3** 193

[8] Gao L L, Lai J W, Chen D, Pei C Y, Wang Q, Zhao Y, Li C H, Cao W Z, Wu J F, Chen Y L, Chen X Q, Sun Y, Felser C, and Qi Y P 2024 *Chin. Phys. Lett.* **41** 057302

[9] Wu F F, Xu Q L, Wang Q Q, Chu Y B, Li L, Tang J, Liu J Y, Tian J P, Ji Y R, Liu L, Yuan Y L, Huang Z H, Zhao J J, Zan X Z, Watanabe K, Taniguchi T, Shi D X, Gu G X, Xu Y, Xian L D, Yang W, Du L J, and Zhang G Y 2023 *Phys. Rev. Lett.* **131** 256201

[10] Xiao D, Yao W, and Niu Q 2007 *Phys. Rev. Lett.* **99** 236809

[11] Xiao D, Liu G B, Feng W, Xu X, and Yao W 2012 *Phys. Rev. Lett.* **108** 196802

[12] Gao A Y, Liu Y F, Hu C W, Qiu J X, Tzschaschel C, Ghosh B, Ho S C, Bérubé D, Chen R, Sun H P, Zhang Z W, Zhang X Y, Wang Y X, Wang N Z, Huang Z M, Felser C, Agarwal A, Ding T, Tien H J, Akey A, Gardener J, Singh B, Watanabe K, Taniguchi T, Burch K S, Bell D C, Zhou B B, Gao W B, Lu H Z, Bansil A, Lin H, Chang T R, Fu L, Ma Q, Ni N, and Xu S Y 2021 *Nature* **595** 521

[13] Mak K F, McGill K L, Park J, and McEuen P L 2014 *Science* **344** 1489

[14] Chen R, Sun H P, Gu M Q, Hua C B, Liu Q H, Lu H Z, and Xie X C 2024 *Natl. Sci. Rev.* **11** nwac140

[15] Zhai D W, Chen C, Xiao C, and Yao W 2023 *Nat. Commun.* **14** 1961

[16] Sinova J, Valenzuela S O, Wunderlich J, Back C H, and Jungwirth T 2015 *Rev. Mod. Phys.* **87** 1213

[17] Orlova N N, Timonina A V, Kolesnikov N N, and Deviatov E V 2023 *Chin. Phys. Lett.* **40** 077302

[18] Oh S 2013 *Science* **340** 153

[19] Sodemann I and Fu L 2015 *Phys. Rev. Lett.* **115** 216806

[20] Li X, Cao T, Niu Q, Shi J, and Feng J 2013 *Proc. Natl. Acad. Sci. USA* **110** 3738

[21] Xu X D, Yao W, Xiao D, and Heinz T F 2014 *Nat. Phys.* **10** 343

[22] Gong Z R, Liu G B, Yu H Y, Xiao D, Cui X D, Xu X D, and Yao W 2013 *Nat. Commun.* **4** 2053

[23] Jones A M, Yu H Y, Ross J S, Klement P, Ghimire N J, Yan J Q, Mandrus D G, Yao W, and Xu X D 2014 *Nat. Phys.* **10** 130

[24] Liu G B, Xiao D, Yao Y G, Xu X D, and Yao W 2015 *Chem. Soc. Rev.* **44** 2643

[25] Du L J, Liao M Z, Liu G B, Wang Q Q, Yang R, Shi D X, Yao Y G, and Zhang G Y 2019 *Phys. Rev. B* **99** 195415

[26] Glazov M M and Golub L E 2020 *Phys. Rev. Lett.* **125** 157403

[27] Du L 2021 *Phys. Rev. Lett.* **127** 149701

[28] Liu Q H, Zhang X W, and Zunger A 2015 *Phys. Rev. Lett.* **114** 087402

[29] Cho S, Park J H, Hong J, Jung J, Kim B S, Han G, Kyung W, Kim Y, Mo S K, Denlinger J, Shim J H, Han J H, Kim C, and Park S R 2018 *Phys. Rev. Lett.* **121** 186401

[30] Du L J, Zhang T T, Liao M Z, Liu G B, Wang S P, He R, Ye Z P, Yu H, Yang R, Shi D X, Yao Y G, and Zhang G Y 2018 *Phys. Rev. B* **97** 165410

[31] Xia J, Yan J X, Wang Z H, He Y M, Gong Y J, Chen W Q, Sum T C, Liu Z, Ajayan P M, and Shen Z X 2021 *Nat. Phys.* **17** 92

[32] Huang Z H, Zhao Y C, Bo T, Chu Y B, Tian J P, Liu L, Yuan Y L, Wu F F, Zhao J J, Xian L D, Watanabe K, Taniguchi T, Yang R, Shi D X, Du L J, Sun Z P, Meng S, Yang W, and Zhang G Y 2022 *Phys. Rev. B* **105** L041409

[33] Du L J, Molas M R, Huang Z H, Zhang G Y, Wang F, and Sun Z P 2023 *Science* **379** eadg0014

[34] Wu F F, Li L, Xu Q L, Liu L, Yuan Y L, Zhao J J, Huang Z H, Zan X Z, Watanabe K, Taniguchi T, Shi D X, Xian L D, Yang W, Du L J, and Zhang G Y 2023 *Chin. Phys. Lett.* **40** 047303

[35] Jacquod P, Whitney R S, Meair J, and Büttiker M 2012 *Phys. Rev. B* **86** 155118

[36] Schaibley J R, Yu H Y, Clark G, Rivera P, Ross J S, Seyler K L, Yao W, and Xu X D 2016 *Nat. Rev. Mater.* **1** 16055

[37] Lee J, Mak K F, and Shan J 2016 *Nat. Nanotechnol.* **11** 421

[38] Zhu B R, Zeng H L, Dai J F, Gong Z R, and Cui X D 2014 *Proc. Natl. Acad. Sci. USA* **111** 11606

[39] Wu Z F, Zhou B T, Cai X B, Cheung P, Liu G B, Huang M Z, Lin J, Han T Y, An L H, Wang Y W, Xu S G, Long G, Cheng C, Law K T, Zhang F, and Wang N 2019 *Nat. Commun.* **10** 611

[40] Zhao Y, Du L, Liang J, Bahramy M, Yang M, Guang Y, Wei Z, Liao M, Tang J, Zhao J, Shen C, Li X, Wang Q, Yang R, Shi D, Liu K, Sun Z, and Zhang G 2020 *Res. Square*

[41] Yuan L D, Liu Q H, Zhang X W, Luo J W, Li S S, and Zunger A 2019 *Nat. Commun.* **10** 906

[42] Zhang K, Zhao S X, Hao Z Y, Kumar S, Schwier E F, Zhang Y J, Sun H Y, Wang Y, Hao Y J, Ma X M, Liu C, Wang L, Wang X X, Miyamoto K, Okuda T, Liu C, Mei J W, Shimada K, Chen C Y, and Liu Q H 2021 *Phys. Rev. Lett.* **127** 126402

[43] Zhang Y J, Liu P F, Sun H Y, Zhao S X, Xu H, and Liu Q H 2020 *Chin. Phys. Lett.* **37** 087105

[44] Zhang X W, Liu Q H, Luo J W, Freeman A J, and Zunger A 2014 *Nat. Phys.* **10** 387

[45] Ryoo J H and Park C H 2017 *NPG Asia Mater.* **9** e382

[46] Wang C, Lian B, Guo X M, Mao J H, Zhang Z T, Zhang D, Gu B L, Xu Y, and Duan W H 2019 *Phys. Rev. Lett.* **123** 126402

[47] Gotlieb K, Lin C Y, Serbyn M, Zhang W T, Smallwood C L, Jozwiak C, Eisaki H, Hussain Z, Vishwanath A, and Lanzara A 2018 *Science* **362** 1271

[48] Ivchenko E L and Pikus G 1997 *Superlattices and Other Heterostructures: Symmetry and Optical Phenomena.* In: *Springer Series in Solid-State Sciences* vol 110 (Springer Science & Business Media)

Supplementary Information: Layer-Valley Hall Effect under Inversion and Time-Reversal Symmetries

Jiaojiao Zhao (赵交交)[1,2], Gui-Bin Liu (刘贵斌)[3,4*], Peng Chen (陈鹏)[5], Yugui Yao (姚裕贵)[3,4], Guangyu Zhang (张广宇)[1,2,6], Luojun Du (杜罗军)[1,2*]

[1]Beijing National Laboratory for Condensed Matter Physics; Key Laboratory for Nanoscale Physics and Devices, Institute of Physics, Chinese Academy of Sciences, Beijing, 100190, China

[2]School of Physical Sciences, University of Chinese Academy of Sciences, Beijing 100190, China

[3]Centre for Quantum Physics, Key Laboratory of Advanced Optoelectronic Quantum Architecture and Measurement (MOE), School of Physics, Beijing Institute of Technology, Beijing 100081, China

[4]Beijing Key Lab of Nanophotonics & Ultrafine Optoelectronic Systems, School of Physics, Beijing Institute of Technology, Beijing 100081, China

[5]Schoolof Microelectronics, Southern University of Science and Technology, Shenzhen 518055, China

[6]Songshan Lake Materials Laboratory, Dongguan, 523808, China

*Corresponding authors. Email: luojun.du@iphy.ac.cn; gbliu@bit.edu.cn

I. The coupling between the combined layer-valley DoF and spin DoF

Figure S1 illustrates the band structures and optical transition selection rules of uncoupled bilayer TMDCs with 2H-stacking[1, 2]. The combined layer-valley configurations $\gamma = \kappa\tau = 1$ ($\gamma = \kappa\tau = -1$) are highlighted by light green (light orange). Because of the strong spin-orbit coupling in valence band, the combined layer-valley DoF is coupled with spin DoF. Specifically, for top valence bands, the layer-valley configurations $\gamma = \kappa\tau = 1$ ($\gamma = \kappa\tau = -1$) are coupled exclusively with spin-up (spin-down). This bears striking resemblance to the coupled valley and spin DoFs in the valence band of monolayer TMDCs[3]. In addition, the optical dipole selection rules are also layer-valley dependent. The interband transitions associated with layer-valley DoF of $\gamma = \kappa\tau = 1$ ($\gamma = \kappa\tau = -1$) are coupled exclusively with σ^+ (σ^-) circularly polarized optical field.

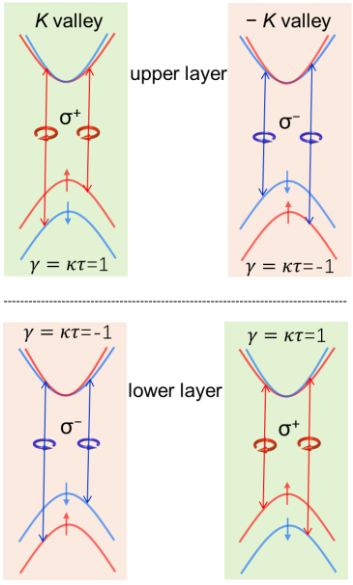

Figure S1. Schematics of band structures and optical transition selection rules of uncoupled bilayer

TMDCs with 2H-stacking. Spin configurations are indicated by ↑ (spin up) and ↓ (spin down). σ^+ (σ^-) denotes left (right) circularly polarized light (circular arrows). Layer-valley configurations $\gamma = \kappa\tau = 1$ ($\gamma = \kappa\tau = -1$) are highlighted by light green (light orange).

II. Spin Hall effect of holes in uncoupled bilayer TMDCs

Because the combined layer-valley DoF is coupled with spin DoF, the layer-valley Hall effect is also accompanied by an intrinsic spin Hall effect. Quantitatively, for moderate hole doping with chemical potential lying between the two-split valence-bands, the intrinsic spin Hall conductivity (in unit of $e/2$) is given by[3]:

$$\sigma_S = 2\int_{BZ}\frac{d^2\boldsymbol{k}}{(2\pi)^2}[f_\uparrow(\boldsymbol{k})\boldsymbol{\Omega}_\uparrow(\boldsymbol{k}) - f_\downarrow(\boldsymbol{k})\boldsymbol{\Omega}_\downarrow(\boldsymbol{k})] = \frac{2}{\pi}\frac{\mu}{\Delta-\lambda} \quad \text{(S1)}$$

where $f(\boldsymbol{k})$ is the equilibrium Fermi-Dirac distribution, μ is the Fermi energy measured from the valence-band maximum, and the integration is performed over the states with layer-valley DoF of $\gamma = 1$. Clearly, the magnitude of intrinsic spin Hall conductivity of holes is the same with that of layer-valley Hall conductivity (equation 3 in the main text) in uncoupled bilayer TMDCs. This is in close resemblance to the coupled valley and spin physics in monolayer TMDCs[3]. It is noteworthy that intrinsic spin Hall effect driven by the Berry phase associated with the Bloch electrons usually requires the spatial-inversion symmetry breaking[4, 5]. The presence of the intrinsic spin Hall effect of equal magnitude to layer-valley Hall effect in uncoupled bilayer TMDCs with inversion symmetry is because of the synergetic effects of layer-valley contrasting Berry curvature and the coupling between spin DoF and the combined DoF.

III. Layer-valley Hall effect for electrons in conduction bands of uncoupled bilayer TMDCs

In close resemblance to valence bands discussed in the main text, each eigenstate $|\tau, s_z\rangle$ in conduction bands is also 100% localized in either upper or lower layer. Consequently, each eigenstate $|\tau, s_z\rangle$ possesses a quantum layer DoF and inherits the nonvanishing Berry curvature $\boldsymbol{\Omega}$ from the constituent upper or lower layer, where the inversion symmetry is intrinsically broken. Quantitatively, the Berry curvature associated with Bloch eigenstate $|\tau, s_z\rangle$ of conduction bands in uncoupled bilayer TMDCs is: $\Omega_c(\tau, s_z) = \nabla_{\boldsymbol{k}} \times \langle\tau, s_z|i\nabla_{\boldsymbol{k}}|\tau, s_z\rangle = -\kappa\tau\Omega_I$, where Ω_I denotes the magnitude of Berry curvature in inversion-asymmetric monolayer TMDCs and is a nearly constant of $\Omega_I = \frac{2a^2t^2}{(\Delta-\lambda)^2}$. Clearly, conduction bands of uncoupled bilayer TMDCs show layer-valley contrasting Berry curvature. For a given layer-valley index, the Berry curvature of conduction band is opposite to that of valence band.

Undoubtedly, the layer-valley contrasting Berry curvature would give rise to layer-valley Hall effect for electrons in conduction bands of uncoupled bilayer TMDCs. In contrast to holes in valence bands with strong spin-orbit coupling, spin-orbit coupling vanishes at the conduction band-edge of ±*K* points and has small spin-splitting quadratic in $\boldsymbol{k}$ ($\boldsymbol{k}$ represents the relative wavevector with respect to the ±*K* points)[3], as shown in Figure S1. As a consequence, for a given layer-valley index $\gamma = \kappa\tau$ with fixed layer index κ and valley index τ, we need to consider both spin-up and spin-down states. In other words, the spin DoF is not coupled to the layer-valley DoF. This bears striking resemblance to the valley Hall effect in monolayer TMDCs, that we must consider both conduction bands[3]. Quantitatively, for moderate electron doping in conduction bands of uncoupled bilayer TMDCs, the layer-valley Hall conductivity (in unit of $e/\hbar$) is given by[3]:

$$\sigma_H^e = 2\int_{BZ}\frac{d^2\boldsymbol{k}}{(2\pi)^2}[f_\uparrow(\boldsymbol{k})\boldsymbol{\Omega}_\uparrow(\boldsymbol{k}) + f_\downarrow(\boldsymbol{k})\boldsymbol{\Omega}_\downarrow(\boldsymbol{k})] = \frac{2}{\pi}\frac{\mu\Delta}{\Delta^2-\lambda^2} \quad \text{(S2)}$$

where $f(\boldsymbol{k})$ is the equilibrium Fermi-Dirac distribution, μ is the Fermi energy measured from the conduction-band minimum, and the integration is performed over the states with layer-valley DoF $\gamma = 1$.

Because for a given layer-valley index $\gamma = \kappa\tau$ with fixed layer index κ and valley index τ, spin-up and spin-down states show small spin-splitting quadratic in $\boldsymbol{k}$, the layer-valley contrasting Berry curvature would also give rise to an intrinsic spin Hall effect. Quantitatively, for moderate electron doping in conduction bands of uncoupled bilayer TMDCs, the spin Hall conductivity (in unit of $e/2$) is given by[3]:

$$\sigma_S^e = 2\int_{BZ}\frac{d^2\boldsymbol{k}}{(2\pi)^2}[f_\uparrow(\boldsymbol{k})\boldsymbol{\Omega}_\uparrow(\boldsymbol{k}) - f_\downarrow(\boldsymbol{k})\boldsymbol{\Omega}_\downarrow(\boldsymbol{k})] = \frac{2}{\pi}\frac{\mu\lambda}{\Delta^2-\lambda^2} \quad \text{(S3)}$$

where $f(\boldsymbol{k})$ is the equilibrium Fermi-Dirac distribution, μ is the Fermi energy measured from the conduction-band minimum, and the integration is performed over the states with layer-valley DoF $\gamma = 1$. In contrast to the hole doped case where spin Hall effect has the same magnitude of conductivity as layer-valley Hall effect, spin Hall conductivity is about λ/Δ of the valley Hall conductivity in electron doped case. λ/Δ is much smaller than 1 and for instance, only ~4% for bilayer MoS_2[1].

IV. Inverse layer-valley Hall effect

In the presence of layer-valley Hall effect, there are both the electrical conductivity σ_{xx} and layer-valley Hall conductivity σ_H. Therefore, the relation between current density $\boldsymbol{j}$ and applied electric field $\boldsymbol{E}$ (in the x-direction) is given by[6]:

$$\begin{pmatrix} j_c \\ j_H \end{pmatrix} = \begin{pmatrix} \sigma_{xx} & -\sigma_H \\ \sigma_H & \sigma_{xx} \end{pmatrix}\begin{pmatrix} E \\ 0 \end{pmatrix} \quad \text{(S4)}$$

where j_c is charge current density along x-direction, and j_H denotes the layer-valley Hall current density in the transverse direction. Based on the equation (S4), an applied electric field can generate a pure layer-valley Hall current in the transverse direction by means of the layer-valley Hall effect: $j_H = \sigma_H E$. Meanwhile, in the light of the Onsager reciprocity relation, the generated layer-valley current can also be converted into an electric field described by:

$$E = \frac{\sigma_H}{(\sigma_{xx})^2+(\sigma_H)^2} j_H \quad \text{(S5)}$$

This can be view as the inverse process of layer-valley Hall effect and refers to inverse layer-valley Hall effect.

V. Layer-valley contrasting orbital magnetic moment

In close analogy to layer-valley contrasting Berry curvature, Bloch electrons in centrosymmetric bilayer TMDCs would also carry a layer-valley contrasting orbital magnetic moment $\boldsymbol{m}$. The orbital magnetic moment is defined by $\boldsymbol{m} = -\left\langle \nabla_{\boldsymbol{k}} u \right| \times \frac{ie}{2\hbar}[H(\boldsymbol{k}) - \varepsilon(\boldsymbol{k})]\left|\nabla_{\boldsymbol{k}} u\right\rangle$, where u is the periodic part of Bloch function, $H(\boldsymbol{k})$ and $\varepsilon(\boldsymbol{k})$ are the Bloch Hamiltonian and band energy, respectively[3, 7]. For Bloch eigenstate $|\tau, s_z\rangle$ in bilayer TMDCs, the orbital magnetic moment is derived as:

$$\boldsymbol{m}(\tau, s_z) = \kappa\tau|\rho|\frac{ea^2t^2(\Delta-\lambda)}{\hbar[(\Delta-\lambda)^2+4a^2t^2k^2]} \quad \text{(S6)}$$

Clearly, layer-valley contrasting orbital magnetic moment exists in real bilayer TMDCs.

VI. Layer-valley dependent optical selection rules

The layer-valley contrasting orbital magnetic moment can give rise to opposite layer-valley angular momentum and thus layer-valley dependent optical dipole selection rules for interband transitions. Specifically, the interband transitions associated with layer-valley DOF $\gamma = \kappa\tau = 1$ ($\gamma = \kappa\tau = -1$) are coupled exclusively with σ^+ (σ^-) circularly polarized optical field, as shown in Figure 1b in the main text. Note that such layer-valley dependent optical dipole selection rules have been experimentally demonstrated in bilayer TMDCs by circular polarization-resolved photoluminescence measurements[8, 9].

[1] Gong Z, Liu G-B, Yu H, Xiao D, Cui X, Xu X and Yao W 2013 *Nat. Commun.* **4** 2053

[2] Du L, Liao M, Liu G-B, Wang Q, Yang R, Shi D, Yao Y and Zhang G 2019 *Phys. Rev. B* **99** 195415

[3] Xiao D, Liu G-B, Feng W, Xu X and Yao W 2012 *Phys. Rev. Lett.* **108** 196802

[4] Manchon A, Koo H C, Nitta J, Frolov S M and Duine R A 2015 *Nat. Mater.* **14** 871

[5] Sinova J, Valenzuela S O, Wunderlich J, Back C H and Jungwirth T 2015 *Rev. Mod. Phys.* **87** 1213

[6] Yamamoto M, Shimazaki Y, Borzenets I V and Tarucha S 2015 *Journal of the Physical Society of Japan* **84** 121006

[7] Xiao D, Yao W and Niu Q 2007 *Phys. Rev. Lett.* **99** 236809

[8] Jones A M, Yu H, Ross J S, Klement P, Ghimire N J, Yan J, Mandrus D G, Yao W and Xu X 2014 *Nat. Phys.* **10** 130

[9] Zhu B, Zeng H, Dai J, Gong Z and Cui X 2014 *Proc. Natl. Acad. Sci. U.S.A.* **111** 11606